Research Square

Preprints are preliminary reports that have not undergone peer review.
They should not be considered conclusive, used to inform clinical practice,
or referenced by the media as validated information.

Preparation and Characterization of CuO/Co3O4/ Poly(Methyl Methacrylate) Nanocomposites Films for Optical and Dielectric Applications

S. El-Sayed
Fayoum University Faculty of Science
Adel El Sayed (ams06@fayoum.edu.eg)
Fayoum University Faculty of Science https://orcid.org/0000-0002-6544-3844

Research Article

Keywords: TMO-PMMA nanocomposites, Co3O4 and CuO Nps, Refractive index, Dielectric relaxation

Posted Date: February 11th, 2021

DOI: https://doi.org/10.21203/rs.3.rs-182788/v1

License: This work is licensed under a Creative Commons Attribution 4.0 International License.
Read Full License

Version of Record: A version of this preprint was published at Journal of Materials Science: Materials in Electronics on April 24th, 2021. See the published version at https://doi.org/10.1007/s10854-021-05949-9.

Preparation and Characterization of CuO/Co_3O_4/ Poly(methyl methacrylate) Nanocomposites Films for Optical and Dielectric Applications

S. El-Sayed[1*], Adel M. El Sayed[1],**

[1]Physics Department, Faculty of Science, Fayoum University, Fayoum 63514, Egypt

Abstract

Composites of transition metal oxides (TMOs)/Polymers have many modern technological, industrial, and biological applications. Co_3O_4 and CuO nanoparticles (Nps) were synthesized by sol-gel. Then they doped into poly(methyl methacrylate) (PMMA) via solution casting method. The obtained Nps and nanocomposite films were then investigated using several techniques. XRD and HR-TEM indicated the high purity of Co_3O_4 and CuO Nps of face-centered cubic (*fcc*) with 58 nm average particle size (D_{av}), and monoclinic structure with D_{av} = 35 nm, respectively. The amorphous nature of PMMA was influenced after mixing with these Nps. SEM and FTIR confirmed the interaction between Nps and the polymer chains. The pure film showed transparency of about 90% and Nps addition narrowed the optical bandgap effectively while keeping the films with high transmittance. CuO is more effective than Co_3O_4 on the optical parameters of the films. The dielectric constant improved after adding the Nps, while all films have a low dielectric loss. Additionally, the effects of Co_3O_4 and CuO on the ac conductivity, Argand plots, and the dielectric modulus are reported. Our nanocomposites are considered a promising candidate for nanotechnology-based devices such as electric stress control, film capacitors and anti-reflective coating for solar cell applications.

Keywords: TMO-PMMA nanocomposites; Co_3O_4 and CuO Nps; Refractive index; Dielectric relaxation.

Corresponding author**: ams06@fayoum.edu.eg (Adel M. **El Sayed), Tel: +201093637986**

1. Introduction

The synthesis of multifunctional materials for utilization in more than one area is attracting increased attention. Transition metal oxides (TMO) and Polymers together have many significant technological applications such as in sensors, optoelectronics, electric vehicles, portable electronic devices, and anticorrosive coatings [1–6]. The enhancement in optical, mechanical, thermal, and electronic properties of nanocomposites is due to the increased surface area/volume ratio, the cooperative phenomena between atoms and molecules, and the quantum confinement effect that occurs in nano-sized materials [7].

Poly(methyl methacrylate), (PMMA; or Plexiglas®), is a transparent polymer, exhibits a low optical absorption and a low index of refraction. It is rigid, mechanically stable, and has high shatter resistance. Also, it is a biocompatible polymer of low-cost and high resistivity to various environmental conditions. Moreover, it exhibits excellent insulating properties with low dielectric loss and small thermal conductivity in the order of 0.2 $Wm^{-1}K^{-1}$ [2,3,8]. These properties make PMMA applicable in fibers, lenses and coatings, implants photoelectrochemical cells, bone cement, in interim-fixed restorations fabrication, as an alternative hard tissue implant [9], contact and intraocular lens, and dental resin, and other biomedical industries [2,7]. Besides, its low dielectric loss makes it the option for dielectric applications such as the dielectric gate for flexible organic field-effect transistors [10]. Based on all these features, PMMA has widely considered the best host material for polymer composites.

To improve and widen its multifunctionality, several working groups have introduced TMO into the PMMA matrix. TiO_2 Nps modified with 3 wt% stearic acids greatly improved the hydrophobicity and anti-icing performance of this polymer. The obtained composite showed a contact angle of 115^o, freezing delay time of 555 s at -10 ^{o}C, and an increase in reflectivity in the visible and near-infrared regions by 57.3% and 42.4%, respectively [11]. Nafee et al.[12] confirmed

that doping of PMMA with Er_2O_3 useful for image sensing, light-emitting diodes (LED), and other nonlinear optical applications. Piramidowicz et al. [13] investigated the UV-blue luminescent features of the sol-gel prepared Tm-doped Y_2O_3 Nps and the spin-coated Y_2O_3:Tm/PMMA films. They found that the active ions were efficiently shielded from the parasitic interactions with the PMMA phonons. Furthermore, M.-Ramírez and R.-Bon applied the sol-gel and dip coating for PMMA/TiO_2 and PMMA/SiO_2 using Eu^{3+} as ion-probe luminescence [14].

Beside the photovoltaics and optoelectronics, the atomic layer deposited PMMA/ZnO nanocomposites are used in wastewater treatment for dye removal [5]. Jang et al. [6] utilized an electroless plating process for the fabrication of FeCoNi@PMMA core-shell structures of lightweight for high-performance electromagnetic-absorbing devices. Mixing 25 wt% of Chitosan/graphene oxide (GO) nano-powder to the PMMA bone cement increased its compressive strength, compressive modulus, and bending strength by 16.2%, 69.1%, and 24.0%, respectively. Hence, the obtained composite can replace commercial bone cement in trauma surgeries and orthopedic devices [15]. Yao et al. [8] reported that the homogeneous dispersion of $Cs_{0.32}WO_3$ Nps inside the PMMA matrix improved its thermal and mechanical properties and led to a high transmittance (>70% in the visible region), a haze in the order of <1%, and excellent blocking ability > 90%, in the wavelength region 780–2600 nm.

Moreover, Ul-Haq et al. [16] reported that loading reduced graphene oxide (rGO) (2.0 wt.%) and Fe_2O_3 (2.0 wt%) inside PMMA increased its dielectric constant (ε') to 308.2 at 25 Hz. Besides the improvement in thermal stability, the thermal conductivity of the ternary composite increased to 2.04 W/mK compared to 1.04 W/mK for 2.0 wt% rGO and 0.98 W/mK for PMMA/2 wt% Fe_2O_3 loadings. Li et al. [3] achieved a significant increase in compressive strength of TiMoCu after using PMMA as filling material to the pores of this alloy. Singh et al. [4] spin-coated PMMA/ZnO films on ITO glass substrates. These films showed a non-volatile electrical bistable behavior (a very close ON and OFF transition voltages) at the ambient temperature. Also, Rajeh et

al. [1] studied the effect of ZnO:Co, at loading ratios less than 1.0 %, on the thermal, structure, and electrical features of PMMA (50%)/PEMA (50%) blend. PMMA loaded with ZrO_2 or TiO_2 nanoparticles exhibited a corrosion resistance in the order of 10^{10} $\Omega \cdot cm^2$ in solution of 3.5% NaCl, that is 7 orders of magnitude greater than that of the bare carbon steel [2].

Among the TMOs, Co_3O_4 is a semiconductor of *p*-type with a spinel structure, environmentally friendly, and has a theoretical capacitance as high as 3560 F/g [17,18]. It is widely used in Li^+ batteries, pseudo-capacitances, dye removal, and field-emission materials [17,19]. Additionally, CuO is a *p*-type semiconductor with E_g in the range of 1.2-2.1 eV [20–22]. CuO shows good thermal and electronic features, index of refraction =1.4, dielectric constant = 18.1 [23]. It is widely used in superconductors & supercapacitors, and solar energy applications [24,25]. Despite all these advantages, no attempts have been reported in the literature to study Co_3O_4/PMMA or CuO/PMMA composites. In this work, the influences of Co_3O_4 and CuO Nps on the optical, structure and electric features of PMMA have been investigated. A sol-gel technique for Nps preparation and solution casting to obtain free-standing films were utilized owing to their low temperature combined with the easy processability, and well-controlled composition for dielectric layers and diverse applications. XRD, HR-TEM, and FTIR have been used to test the crystal and chemical structure of the films. The optical and dielectric parameters of the composite films are discussed in detail.

2. Experimental Procedures

2.1. Chemicals

Cobalt nitrate, $Co(NO_3)_2.6H_2O$, of high purity and molecular weight M_W = 291.03 g/mol, from Fluka, copper acetate, $Cu(CH_3COO)_2.H_2O$, of high purity and M_W = 199.65 g/mol from Barcelona, PRS Panreac, and high purity oxalic acid, $C_2H_2O_4.2H_2O$, of M_W = 126.07, from Loba Chemie, India, were used for Co_3O_4 and CuO Nps synthesis. PMMA of M_W = 25,000 g/mol, from Poly Science, Warrington, PA, USA and chloroform, $CHCl_3$, of M_W = 119.38 g/mol, were used for films' preparation.

2.2. Methods

A solution of 0.75 M was prepared by dissolving 21.83 *g* of cobalt nitrate in 100 *ml* distilled water (DW) using a magnetic stirring. About 14.2 g of oxalic acid was dissolved in 100 *ml* water and mixed with the first solution by stirring for 1.0h at ~ 60 ^{o}C. A similar oxalic acid solution was added to a 0.75 M solution prepared by dissolving the required amount of copper acetate in DW. The obtained Co and Cu solutions were aged for one day at room temperature (*RT*). The final gels were calcined at 450 ^{o}C for 2.0 h in an air furnace, then left to cool naturally to RT. After grounding the powders, they were kept in zipper bags to eliminate the moisture. The pure (reference) film was prepared by dissolving 1.0 g PMMA powder in 50 ml $CHCl_3$ in a tightly closed beaker using magnetic stirring for 2.0 h. Similar procedures were applied for preparing the nanocomposites. The required masses of Co_3O_4 and CuO were loaded, under vigorous stirring at RT, into the PMMA solution to obtain PMMA film loaded with 0.05%, 0.10% Co_3O_4, (0.10% CuO + 0.10% Co_3O_4), (0.50% CuO + 0.10% Co_3O_4), (1.0% CuO + 0.10% Co_3O_4). The composite solutions were put into glass Petri dishes. These dishes are left to dry at RT for one day. Free-standing films free from any solvent traces were carefully peeled off the dishes. The films' thickness was measured by a digital micrometer and found to be in the range of 0.1 - 0.3 mm.

2.3. Measurements

Fourier transform infrared (FTIR) spectra were recorded by Spectrophotometer, Nicolet iS10, USA, at RT in 400-4000 cm^{-1} wavenumbers range. X-ray diffraction patterns of nanoparticles and films were scanned at 4.0^{o} – 80^{o} via XRD, PANalytical X'PertPRO, with Cu K_α radiation (λ = 1.5406 Å). Transmission electron microscopy of high resolution, JEM 2100, Jeol, Japan, was used to investigate the morphology and the particle size of Co_3O_4 and CuO NPs. Scanning electron microscopy (SEM), Inspect S, FEI, Holland was used to investigate the surface morphology of pure and nanocomposite films. UV–vis spectra were recorded, using a JASCO 630 spectrophotometer, in 190–1600 nm wavelength (λ) range. To evaluate E_g of the prepared Nps, the absorption spectrum (*Abs.*) was recorded using a solution of 2.5 mg nano-powder in 50 *ml* ethanol. The coefficient of absorption (α) was calculated using the follwoing relation [19, 26];

$$\alpha = [2.303\, x10^{-3}(Abs.).\rho]/(l.\gamma) \quad (1)$$

where ρ is the density of Nps (6.2 and 6.31 g/cm^3 for Co_3O_4 and CuO, respectively [27,28], l is the optical path length, and γ is the concentration. The dielectric properties of the prepared films were

performed using a high tester LCR meter bridge, Hikoi, model 3532, Ueda, Nagano, Japan, in 0.1 Hz – 10.0 MHz frequency range, with an accuracy of $\pm 1 \times 10^{-4}$ pF for C_p measurement.

3. Results and discussions

3.1. Structural Properties

3.1.1. FTIR

FTIR is an important technique to check the interactions and complexation between the added TMOs NPs and the functional groups of the polymer. The curves are displayed in Fig. 1. The two adjacent bands at 2995 cm^{-1} and 2952 cm^{-1} denote the stretching vibration of methyl ($–CH_3$) and methylene ($=CH_2$) groups [3] that diminish gradually by increasing the dopants concentration. The carbonyl (C=O) group and C–O group are the fingerprint characteristic bands of PMMA and their stretching vibrations appSear at 1731 and 1442 cm^{-1}, respectively. The small band at 1391 cm^{-1} is attributed to CH_3 deformation [16]. The vibration bands at 1245 cm^{-1} and the strong one at 1146 cm^{-1} are due to the ether (C–O–C) group of PMMA [3,29]. Moreover, vibrations of –CH=CH group (at 980 cm^{-1}) and the waging vibrations of C–H in the $–CH_3$ groups (at 841 cm^{-1}) are characteristic wavenumbers of PMMA [9]. Finally, the bands at 748 and 480 cm^{-1} are assigned to C-H bending [30].

Increasing the dopants' content led to a decrease in the peaks' intensity and sharpness of the bands. This demonstrates the relatively strong bonding associated with the deep interactions of Co–O & Cu–O inside the PMMA matrix. However, the interactions of CuO with PMMA seem stronger compared to Co_3O_4. The M_W of Co_3O_4 ≈ 240.79 and M_W of CuO ≈ 79.55 g/mol. Equal masses of Co_3O_4 and CuO give a different number of moles, i.e. the number of moles of 0.1 wt.% CuO to that of 0.1 wt.% Co_3O_4 is equal to 3.03: 1.0. So that, the higher mole number of CuO supports the intense interactions with the polymer chains.

3.1.2. XRD

X-ray diffraction patterns of PMMA, Co_3O_4/PMMA, and CuO/Co_3O_4/PMMA nanocomposite films are shown in Fig. 2. The spectrum of PMMA (un-doped film) shows three peaks at 2θ = 14.29°, 30.41°, and 41.89°, that are broad and indicate the semicrystalline feature of PMMA or existance of wrong ordering [31]. A comparable XRD pattern was found for PMMA film prepared by ball milling [9]. Another research group found these broad peaks for pure PMMA at ~ 13.86°, 29.42°, and 42.33° [29]. Additionally, Ul-Haq et al.[16] found the three broad peaks at 15°, 30° and 45° for PMMA synthesized during in-situ polymerization using MMA monomers. Loading 0.05% Co_3O_4 depressed these peaks. Increasing this ratio to 0.1% results in the appearing of peaks at 2θ = 31.12°, 36.71°, 65.20° which are due to Co_3O_4 of *fcc* structures according to JCPDS file No. 78-1970. These peaks are superimposed on PMMA peaks. Singh et al. [4] reported a peak at 13.8° in the diffraction patterns of PMMA/ZnO composite related to PMMA. Codoping with CuO Nps is confirmed through the appearance of several peaks for monoclinic CuO with a = 4.685Å, b = 3.43Å, c =5.13 Å and β = 99.55°, according to JCPDS file no. 45-0937. The peak's intensity increases with increasing CuO content from 0.1 to 1.0%, where the most intense peaks are at 2θ = 32.31°, 35.35°, 38.55°, 48.58°, and 53.05°. The PMMA' peaks gradually reduced and depressed in intensity with doping, except at 0.1% Co_3O_4 and 1.0% CuO & 0.1% Co_3O_4. This indicates the deep interactions between Co_3O_4 & CuO with PMMA functional groups.

Miller's indices of Co_3O_4 and CuO are mentioned above their XRD peaks, as shown in Fig. 2. The crystallite size of these Nps was calculated using Scherer's formula, $D= (0.89\lambda/FWHM\ cos\theta)$, where λ = 0.154 nm is the applied wavelength, and *FWHM* denotes the full width at half maximum intensity. The D value of Co_3O_4 is ranged from 36.3 to 79.8 nm with an average $D_{av} \approx 58$ nm. The D values of CuO are in the range, 17.8 – 52.2 nm, with D_{av} = 35 nm. To investigate the morphology and check the size of the sol-gel prepared Nps, HR-TEM images were taken for these Nps, as shown in Fig. 3. As seen, Co_3O_4 Nps seem larger than CuO Nps. The measured sizes by this

instrument are larger than those calculated from XRD data (the size of crystals). This illustrates that electron microscopy gives the visual particle (grain) size by measuring the distances between the grain boundaries. Thus, more than one crystallite are contained in each grain.

3.1.3. SEM

To study the PMMA's surface morphology, the distribution and dispersion of the added Nps on its surface, SEM images were taken for un-doped PMMA, Co_3O_4/PMMA, and CuO/ Co_3O_4/PMMA composite films, and displayed in Fig. 4 (a–f). The surface of PMMA is a nonporous crimped or networked structure. Nps addition disturbed the wavy morphology of PMMA. Co_3O_4 Nps are uniformly distributed, however, increasing CuO Nps content result in small numbers of agglomerated particles.

3.2. Optical features

The recorded transmittance (*T%*) spectra of pure and nanocomposite films are presented in Fig. 5. In the region where $\lambda < 300$ nm, a sharp increase is seen in *T%* for all films. In the region $\lambda > 300$ nm, the undoped film exhibit 80% transmittance increases to ~ 92% with increasing λ of the incident photon to 1570 nm. Loading 0.1% Co_3O_4 lower this limit to ~ 82% and mixing with 1.0% CuO Nps greatly reduced it to 43%. This reduction in *T%* appears in the inset of Fig. 5 in $242 > \lambda > 295$ nm. Increasing Nps content inside PMMA increased the scattered number of the incident photons and led to the observed decrease in *T%*. However, the obtained *T%* values encourage using these composite films for optical coating purposes [31]. Using the recorded absorption (*Abs.*) spectra and measuring the films' thickness (*d*) by a digital micrometer, as listed in Table 1, both the absorption coefficient ($\alpha = 2.303\ Abs./d$) and the extinction coefficient ($k = \alpha\lambda/4\pi$) were determined. There is a sharp increase in the *k* spectra below 240 nm wavelength, as displayed in Fig. 6. It corresponds to the $\pi \rightarrow \pi^*$ transition of PMMA C=O groups. The relatively small absorbance band displayed around 275 nm owing to the $n \rightarrow \pi^*$ transitions induced by the un-

bonded electrons. Change the peaks' position to longer λ with doping confirms the complexation between Nps and the polymeric chains. For pure PMMA, there is a reduction in the absorption spectra in the 235–300 wavelength range, while at higher λ they become stable. This indicates the transparent nature of the freestanding PMMA film to the whole visible wavelength over 300 nm. The k values of the composite films increase linearly with λ in the high λ side. In almost all range of λ, k values are less than 2 x 10^{-4}, and the very low values confirm the transparent nature of the composite films.

The *Abs.* spectra of Co_3O_4 and CuO Nps are depicted in Fig. 7. Co_3O_4 Nps exhibit two small and broad absorption bands centered around 445 and 750 nm, while CuO Nps have one sharp absorption band at 340 nm. It is known that the band's position depends on the D value of the synthesized Nps [21]. The *Abs.* spectra were used to calculate α as given by equation 1. The direct optical bandgap (dE_g) of these Nps were determined by plotting $(\alpha h\upsilon)^2$ vs. the photon energy ($h\upsilon$). As seen in the inset of Fig. 7, extending of the linear part to zero absorption yields the dE_g values. Two dE_g for the Co_3O_4 Nps, the first one is dE_{gI} =1.385 eV, and the second is dE_{gII} =1.91 eV. $\Delta E_g = dE_{gII} - dE_{gI}$ = 0.53 eV. Comparable values were found for Co_3O_4 [18,19,27]. The dE_{gII} is the true bandgap energy and owing to interband transition. Whereas dE_{gI} is correlating to the beginning of excitations of $O^{-2} \rightarrow Co^{+3}$. The estimated dE_g value for the second oxide is ~ 2.2 eV, compatible with the previously published data [20,21].

The added Nps cause the PMMA absorption edge to shift in the low hυ side. Both dE_g and iE_g (indirect optical band gap) of the composite films were evaluated utilizing Tauc's model; $(\alpha h\upsilon)^2 = B(h\nu - dE_g)$ and $(\alpha h\upsilon)^{\frac{1}{2}} = A(h\nu - iE_g)$ [32], $B = 4\pi c\sigma_o/n_o E_U$, where σ_o n_o, and E_U are the electrical conductivity, the refractive index at absolute zero and Urbach energy, respectively. Fig. 8 (a, b) represents the reliance of $(\alpha h\upsilon)^2$ and $(\alpha h\upsilon)^{1/2}$ on $h\upsilon$. The values of dE_g and iE_g were obtained by extending the linear regions of $(\alpha h\upsilon)^2$ & $h\upsilon$ and $(\alpha h\upsilon)^{1/2}$ & $h\upsilon$ plots to α = 0. The obtained results are given in Table 1. As seen, dE_g and iE_g of PMMA decreased from 4.80 eV and

4.45 eV to 4.60 eV and 4.35 eV after loading 0.1% Co_3O_4 Nps, and this decrease continued to 4.30 eV and 4.08 eV after codoping with CuO Nps. Similarly, loading Er_2O_3 Nps at 8% decrease the dE_g of PMMA from 5.39 to 5.13 eV [12]. As mentioned in the previous paragraph, E_g of Co_3O_4 and CuO Nps are 1.91 and 2.2 eV, which are smaller than both dE_g and iE_g of PMMA. Thus, the oxides can create charge-transfer complexes and induced defects in the polymer. These modifications in the film's band structure are reflected by the drop in the absorption edge with Nps addition that creates new localized states within the bandgap [30]. The width of these localized states is the Urbach tail, the value of E_U is determined by utilizing the equation [32]: $\alpha = \alpha_o e^{(E-E_I/E_U)}$, where E_I and α_o are constants. Fig. 9 shows the $ln(\alpha)$ vs. $h\upsilon$ plots for the composite films, where E_U values are the reciprocal of the straight lines of these curves, i.e. $E_U=1/(\Delta(ln\alpha)/\Delta h\upsilon)$. The E_U values are tabulated in Table 1. E_U values increase from 161 to 182 and to 201 meV after doping with 0.1% Co_3O_4 and codoping with 1.0% CuO Nps. Thus the complexations between PMMA and these Nps increases the disorder and defects inside PMMA. This cause reduction in dE_g and iE_g value of the polymer and encourage the segmental motion of their chains. Therefore, Nps addition facilitates the diffusion of ions between valence and conduction bands of PMMA, and it is expected to improve its electrical conductivity.

The optical constant of the transparent materials, especially the refractive index (n), is an essential parameter in designing of the optical device. The value of n is determined using the recorded reflectance spectra (R) and the determined values of k by using the following equation [33]: $n = \frac{(1+R)+(4R-(1-R)^2k^2)^{1/2}}{(1-R)}$. Fig. 10 shows the n values of the films with λ. In the region λ ≈ 300 nm, PMMA has n values equal 1.6 – 2.25 increase to be in the range 3.1 – 4.0 after Nps addition. The results mean that n is inversely proportional to both dE_g and iE_g. Similarly, Beltran et al. [34] reported that n = 1.56 at λ = 532 nm for PMMA loaded with ZrO_2. The increased n values after doping suggest using these nanocomposite films as high n lenses and for antireflection coating

for solar cell applications. The dispersion equation [33]: $n^2 = \varepsilon_l - \lambda^2 \left(\frac{e^2}{\pi c^2}\right)\left(\frac{N}{m^*}\right)$ could be used to determine the lattice dielectric (ε_l) constant and the carriers concentration/the effective mass of the electron, i.e. $\left(\frac{e^2}{\pi C^2}\right)\left(\frac{N}{m^*}\right)$. This is achieved by plotting the dependence of n^2 on λ^2, as given in the inset of Fig. 10, and the obtained values are tabulated in Table 1. The values of ε_l and $\left(\frac{e^2}{\pi C^2}\right)\left(\frac{N}{m^*}\right)$ are slightly increased from 3.7 to 3.8 and from 4.95 x 10^{-5} to 5.93 x 10^{-5}, respectively, by doping with 0.1% Co_3O_4 Nps. These values, however, significantly increased to be in the range of 6.7–10.4 and 6.85 x 10^{-5} – 10.51 x 10^{-5}, with increasing the codoped ratios of CuO Nps in the range 0.1 – 1.0%. This indicates that CuO is more effective on the optical constants of PMMA. Also, the obtained result agrees with the changes in dE_g and iE_g, where increasing carrier concentration, the E_{gs} is expected to be narrower.

3.3. Electric properties

The reliance of the dielectric constant (ε') of pure and TMOs-doped PMMA on the angular frequency (ω) in 293–383K range of temperatures is depicted in Fig. 11 (a–f). It is seen that the TMOs-doped films have higher ε' compared with the un-doped film. The ε' values increase with increasing temperature, especially at 383 K, and decrease with increasing ω. At 293 K (room temerature), ε' of PMMA is between 1.5 –1.9 and this range increased to 2.3 – 3.6 at 383 K. Loading 0.1% Co_3O_4 resuilt in increasing ε' to be in the range 2.4 – 3.0 (at 293 K) and 3.0 – 5.0 (at 383 K). Furthermore, codoping with 1.0% CuO raised this range to 3.4 – 4.1 (at 293 K) and 4.2 – 8.0 (at 383 K).

At small values of ω, the greater ε' values coming from various kinds of polarization; interfacial, ionic, atomic and electronic. At higher *f* values, only two kinds can exist; electronic and atomic polarization. At first, the dipoles can follow the applied *f* but let down (can't reorient themselves in the electric field direction at higher values) due to the decreased period. The

improvements in ε' values for the doped films arise from the high permittivities of the used oxides [23]. Doping with the oxides could encourage the PMMA's functional groups to have ordered states which affect the material's polarization. Moreover, the uniform distribution of the Nps on the PMMA surface facilitates the transportation of the charge carriers', resulting in higher values for ε' [35].

Fig. 12 (a–f) displays the dielectric loss (ε'') of PMMA, Co_3O_4/PMMA, and CuO/Co_3O_4/PMMA films. Within the studied range of applied frequencies (0.25 Hz – 7.30 MHz) and temperatures (293 – 383K), all samples have ε'' in the range 0.05 – 0.43. Clear relaxation peaks are seen in the spectra of ε''. The higher ε'' values at the relaxation peak (ε''_{max}) are listed in Table 2. For each film, these peaks are shifted to higher frequencies as the temperature increased. The heating process results in a free volume increment and hence facilitates the chain segment orientation and chain dynamics [36]. At 293 – 323 K, All films have low ε'' values and these values irregularly changed with increasing dopants content. However, these values become higher at elevated temperatures (353 – 383 K) and also increased with doping, i.e. raising the temperature beyond 323 K has the decisive effect on ε''. The nanocomposite films have enhanced ε' (this means a higher dielectric displacement and a high energy density) and low ε''. This encourages the use of these films in thin-film capacitors and some other applications such as in devices of the electric stress control [37].

The electric conductivity of the samples was calculated utilizing the equation: $\sigma_{ac} = \omega\varepsilon_o\varepsilon''$ and the obtained values are shown in Fig. 13 (a–f). Also, the values of σ_{ac} at 1.0 MHz and two selected temperatures (323 and 383 K) are given in Table 2. For all films, σ_{ac} is in the order of 10^{-6} – 10^{-5} S/cm. At $f < 10^4$ Hz, there no observed change in σ_{ac} whatever the temperature or the dopant ratios, i.e. σ_{ac} is constant. At 323 K and 1.0 MHz, σ_{ac} increases from 1.06 x 10^{-6} to 1.97 x 10^{-6} S/cm after loading 0.1% Co_3O_4 and significantly increased to 4.18 x 10^{-6} S/cm after the additional

loading with CuO. The corresponding values of σ_{ac} at 383 K and 1.0 MHz are 5.84 x 10^{-6}, 1.65 x 10^{-5} and 4.67 x 10^{-5} S/cm. The increase in σ_{ac} after $f \geq 10^4$ Hz and the little influence of temperature, at T ≤ 353 K, indicating that the mobility of the carriers are governed by hopping over the defects along the polymer bonds [38]. The uniform distribution of Co_3O_4 and CuO inside PMMA forms several 3D conductive networks, assisting the charges to hop from one cluster to its neighbors.

This subsection is devoted to studying the nature of electric transport and the relaxation mechanism in our samples. The real M' and M'' dielectric modulus can be determined as $M' = \frac{\varepsilon'}{\varepsilon'^2+\varepsilon''^2}$ and $M'' = \frac{\varepsilon''}{\varepsilon'^2+\varepsilon''^2}$. Fig. 14 (a–f) depicts the relation between M'' of the films and f at 293 – 383 K. At 293 – 353 K, the small M'' value at the smallest f values means that the polarization effects between the film and the electrode are negligible. Such an effect appears at a higher temperature (383 K) and is owing to the high capacitance linked to the electrodes [39]. M'' value increases until an utmost value at some f value. This arising from random hopping of long-range for charge carriers. The observer peaks are attributed to a relaxation phenomena as the motion of long-range is converted to a confined one. After that, with the continuous increment in the frequency, M'' values tend to be lower. This indicates that the charges became in a potential well, and brief distances are only alloyed. Heating at 293 – 383 K cause shifting for these peaks to higher f value. Thus increasing temperatures decreases the strength of the polymer chains and increases their segmental dynamic motion. In general, the doped PMMA films have more wide peaks for M'' at smallest values for M''_{max}. This illustrates a plurality of relaxation mechanisms.

Additionally, Argand (Cole-Cole) plots for un-doped and TMOs-doped PMMA are depicted in Fig.15. All curves seem to be semicircles with their centers not on M' axis. This suggests that the process of relaxation in these films are of non-Debye one [35]. With increasing the temperatures from 293 to 383 K, the M'' peak positions are shifted to a higher M'', and in general,

the peaks are shifted to lower M' values (left-shift). Besides, TMOs-doped films have broader peaks with lower intensity regarding PMMA. These results demonstrate the effective nature of Co_3O_4 and CuO Nps on the dielectric properties and relaxation phenomena of PMMA.

4. Conclusion

Nanocomposites based on CuO/ Co_3O_4/PMMA were fabricated by casting technique. The effect of doping with Co_3O_4 Nps and codoping with CuO Nps on the PMMA' properties were discussed. FTIR spectra illustrated the formation of PMMA based nanocomposite films. CuO Nps interact strongly with PMMA compared to Co_3O_4. XRD confirmed the amorphous nature of PMMA. Co_3O_4 has *fcc* structures, D_{av} = 58 nm, and basic bandgap energy dEg = 1.91 eV. While CuO crystallizes in monoclinic structure with D_{av} = 35 nm, and dE_g value of ~ 2.2 eV. SEM analysis showed that PMMA has a surface of a crimped structure and Co_3O_4 and CuO Nps dispersed homogeneously on the polymer surface. PMMA exhibits transparency in the range 80 – 92% but reduced after doping. The two absorption bands in the spectra of the k parameter at 240 and 275 nm correspond to $\pi \rightarrow \pi^*$ and $n \rightarrow \pi^*$ electronic transitions. The direct and indirect bandgap (dE_g and iE_g) of PMMA decreased from 4.80 eV and 4.45 eV to 4.60 eV and 4.35 eV after loading 0.1% Co_3O_4 Nps and this decrease continued to 4.30 eV and 4.08 eV after codoping with CuO Nps. The related increase in E_U parameter was from 161 to 201 meV. PMMA has n = 1.6 – 2.25 increase to be in the range 3.1 – 4.0 after Nps addition. The carriers concentration/the effective mass of the electron increased from 4.95 x 10^{-5} to 5.93 x 10^{-5} by doping with 0.1% Co_3O_4 Nps and 6.85 x 10^{-5} after codoping with 0.1% CuO. Therefore, CuO Nps is widely effective for controlling or adjusting the optical constants of PMMA. The dielectric constant (ε') of PMMA significantly increased from 1.5 –1.9 to be in the range of 4.2 – 8.0 due to doping and heating processes, while the dielectric loss remains almost very low. The electric conductivity (σ_{ac}) at 383 K and 1.0 MHz are 5.84 x 10^{-6}, 1.65 x 10^{-5} and 4.67 x 10^{-5} S/cm, for pure, 0.1% Co_3O_4 and 1.0% CuO + 0.1% Co_3O_4 loadings. The spectra of dielectric modulus and Argand plots suggest that the relaxation processes in these films follow non-Debye

model. These results encourage the utilization of our nnaocomposite films in some applications such as in capacitors and energy storage applications, devices of electric stress control, and antireflective coating for solar cells.

Declaration of interests

The authors declare that they have no known competing financial interests or personal relationships that could have appeared to influence the work reported in this paper.

There are no interests to declare towards any financial interests/personal relationships which may be considered as potential competing interests.

5. References

[1] A. Rajeh, H.M. Ragab, M.M. Abutalib, *"*Co doped ZnO reinforced PEMA/PMMA composite: Structural, thermal, dielectric and electrical properties for electrochemical applications*", J. Molec. Struct.* vol. 1217, pp. 128447, 2020.

[2] S.V. Harb, A. Trentin, M.C. Uvida, M. Magnani, S.H. Pulcinelli, C.V. Santilli, P. Hammer, "A comparative study on PMMA-TiO_2 and PMMA-ZrO_2 protective coatings", *Progr. Organ. Coat.*, vol. 140, pp. 105477, 2020.

[3] Y.-H. Li, X.-Y. Shang, Y.-J. Li, "Fabrication and characterization of TiMoCu/PMMA composite for biomedical application", *Mater. Lett.*, vol. 270, pp. 127744, 2020.

[4] S.P. Singh, S.K. Sharma, D. Y. Kim, "Carrier mechanism of ZnO nanoparticles-embedded PMMA nanocomposite organic bistable memory device", Solid State Sciences vol. 99, pp. 106046, 2020.

[5] A.D. Mauro, C. Farrugia, S. Abela, P. Refalo, M. Grech, L. Falqui, V. Privitera, G. Impellizzeri, "Synthesis of ZnO/PMMA nanocomposite by low-temperature atomic layer deposition for possible photocatalysis applications", *Mater. Sci. Semicond. Process.*, vol. 118, pp. 105214, 2020.

[6] W. Jang, S. Mallesh, S.B. Lee, K.H. Kim, "Microwave absorption properties of core-shell structured FeCoNi@PMMA filled in composites", *Curr. Appl. Phys.*, vol. 20, 525–530, 2020.

[7] Z.G. Ayanoğlu, M. Doğan, "Characterization and thermal kinetic analysis of PMMA/modified-MWCNT nanocomposites", *Diamond & Related Mater.*, vol. 108, pp. 107950, 2020.

[8] Y. Yao, Z. Chen, W. Wei, P. Zhang, Y. Zhu, Q. Zhao, K. Lv, X. Liu, Y. Gao, "$Cs_{0.32}WO_3$/PMMA nanocomposite via in-situ polymerization for energy saving windows", *Solar Energy Mat. Sol. C.* vol. 215, pp. 110656, 2020.

[9] I. Chrysafi, E. Kontonasaki, A.D. Anastasiou, D. Patsiaoura, L. Papadopoulou, G. Vourlias, E. Vouvoudi, D. Bikiaris, "Mechanical and thermal properties of PMMA resin composites for interim fixed prostheses reinforced with calcium β-pyrophosphate", *J. mechan. behav. biomed. mater.,* vol. 112, pp. 104094, 2020.

[10] G.P. Viorica, V. Musat, A. Pimentel, T.R. Calmeiro, E. Carlos, L. Baroiu, R. Martins, E. Fortunato, "Hybrid (Ag)ZnO/Cs/PMMA nanocomposite thin films" *J. Alloy Compds.*, vol. 803, pp. 922-933, 2019.

[11] Y. Xi, Y. Qi, Z. Mao, Z. Yang, J. Zhang, "Surface hydrophobic modification of TiO_2 and its application to preparing PMMA/TiO_2 composite cool material with improved hydrophobicity and anti-icing property", *Construc. Build. Mater.*, vol. 266, pp. 120916, 2021.

[12] S.S. Nafee, T.A. Hamdalla, A.A.A. Darwish, "Studies of the morphology and optical properties of nano erbium oxide embedded in PMMA matrix", *Opt. Laser Technol.*, vol. 129, pp. 106282, 2020.

[13] R. Piramidowicz, A. Jusza, L. Lipinska, M. Baran, P. Polis, A. Olszyna, "UV-blue luminescent properties of Tm^{3+}:Y_2O_3 nanocrystals and PMMA-based composites", *J. Luminesc.*, vol. 226, pp. 117458, 2020.

[14] M.L. M.-Ramírez, R. R.-Bon, "Microstructural comparison between PMMA-SiO_2 and PMMA-TiO_2 hybrid systems using Eu^{3+} as ion-probe luminescence", *J. Non-Crystall. Solids*, vol. 544, pp. 120167, 2020.

[15] M. Tavakoli, S.S.E. Bakhtiari, S. Karbasi, "Incorporation of chitosan/graphene oxide nanocomposite in to the PMMA bone cement: Physical, mechanical and biological evaluation", *Int. J. Biolog. Macromol.*, vol. 149, 783–793, 2020.

[16] Y. Ul-Haq, I. Murtaza, S. Mazhar, R. Ullah, M. Iqbal, Z. Ui-Huq, A.A. Qarni, S. Amin, "Dielectric, thermal and mechanical properties of hybrid PMMA/RGO/Fe_2O_3 nanocomposites fabricated by in-situ polymerization", *Ceram. Int.*, vol. 46, pp. 5828−5840, 2020.

[17] G.A.M. Ali, O.A. Fouad, S.A. Makhlouf, "Structural, optical and electrical properties of sol–gel prepared mesoporous Co_3O_4/SiO_2 nanocomposites", *J. Alloys Compds.*, vol. 579, pp. 606–611, 2013.

[18] K. Deori, S.K. Ujjain, R.K. Sharma, S. Deka, "Morphology Controlled Synthesis of Nanoporous Co_3O_4 Nanostructures and Their Charge Storage Characteristics in Supercapacitors", *ACS Appl. Mater. Interfaces*, vol. 5, pp. 10665−10672, 2013.

[19] S.A. Makhlouf, Z.H. Bakr, K.I. Aly, M.S. Moustafa, "Structural, electrical and optical properties of Co_3O_4 nanoparticles", *Superlat. Microstruc.*, vol. 64, pp. 107–117, 2013.

[20] F.K. Mugwang'a, P.K. Karimi, W.K. Njoroge, O. Omayio, S.M. Waita, "Optical characterization of Copper Oxide thin films prepared by reactive dc magnetron sputtering for solar cell applications", *Int. J. Thin Film Sci. Tech.*, vol. 2, pp. 15–24, 2013.

[21] B.G. Ganga, P.N. Santhosh, "Manipulating aggregation of CuO nanoparticles: Correlation between morphology and optical properties", *J. Alloys Compd.*, vol. 612, pp. 456–464, 2014.

[22] Y.S. Chaudhary, A. Agrawal, R. Shrivastav, V.R. Satsangi, S. Dass, "A study on the photoelectrochemical properties of copper oxide thin films", *Int. J. Hydrogen Energ.*, vol. 29, pp. 131–134, 2004.

[23] Q. Zhang, K. Zhang, D. Xu, G. Yang, H. Huang, F. Nie, C. Liu, S. Yang, "CuO Nanostructures: Synthesis, Characterization, Growth Mechanisms: Fundamental Properties and Applications", *Prog. Mater. Sci.*, vol. 60, pp. 208–337, 2014.

[24] Y.X. Zhang, M. Huang, F. Li, Z.Q. Wen, "Controlled Synthesis of Hierarchical CuO Nanostructures for Electrochemical Capacitor Electrodes", *Int. J. Electrochem. Sci.*, vol. 8, pp. 8645–8661, 2013.

[25] H. Zhu, F. Zhao, L. Pan, Y. Zhang, C. Fan, Y. Zhang, J.Q. Xiao, "Structural and magnetic properties of Mn-doped CuO thin films", *J. Appl. Phys.*, vol. 101, pp. 09H111, 2007.

[26] V. Patil, P. Joshi, M. Chougule, S. Sen, "Synthesis and Characterization of Co_3O_4 Thin Film", *Soft Nanosci. Lett.*, vol. 2, pp. 1–7, 2012.

[27] A.M. El Sayed, S. El-Gamal, "Synthesis and investigation of the electrical and dielectric properties of Co_3O_4/(CMC+PVA) nanocomposite films", *J. Polym. Res.*, vol. 22, pp. 97, 2015.

[28] A.M. El Sayed, S. El-Gamal, W.M. Morsi, G. Mohammed, "Effect of PVA and copper oxide nanoparticles on the structural, optical, and electrical properties of carboxymethyl cellulose films", *J. Mater. Sci.*, vol. 50, pp. 4717–4728, 2015.

[29] A. Abun, B.-R. Huang, A. Saravanan, D. Kathiravan, P.-D. Hong, "Effect of PMMA on the surface of exfoliated MoS_2 nanosheets and their highly enhanced ammonia gas sensing properties at room temperature", *J. Alloy Compds.*, vol. 832, pp. 155005, 2020.

[30] S.B. Aziz, O.G. Abdullah, M.A. Brza, A.K. Azawy, D.A. Tahir, "Effect of carbon nano-dots (CNDs) on structural and optical properties of PMMA polymer composite", *Res. Phys.* vol. 15, pp. 102776, 2015.

[31] A.M. El Sayed, "Aspects of structural, optical properties, and relaxation in ($BiFeO_3$ or $NaTiO_3$)–PMMA: Hybrid films for dielectric applications", *J. Phys. Chem. Solids*, vol. 148, pp. 109767, 2021.

[32] A.M. El Sayed, S.Taha, G.Said, F.Yakuphanoglu, "Controlling the structural and optical properties of nanostructured ZnO thin films by cadmium content", *Superlattice Microstruct.*, vol. 65, pp. 35–47, 2014.

[33] M. Shaban, A.M. El Sayed, "Influence of the spin deposition parameters and La/Sn double doping on the structural, optical, and photoelectrocatalytic properties of $CoCo_2O_4$ photoelectrodes", *Solar Energy Mater. Sol. C.,* vol. 217, pp. 110705, 2020.

[34] C.G. A.-Beltran, J.L. A.-Sanchez, R. R.-Bon, "Synthesis and properties of PMMA-ZrO_2 organic–inorganic hybrid films", *J. Appl. Polym. Sci.,* vol. 132, pp. 42738, 2015.

[35] A.M. El Sayed, G. Khabiri, "Spectroscopic, Optical and Dielectric Investigation of (Mg, Cu, Ni, or Cd) Acetates' Influence on Carboxymethyl Cellulose Sodium Salt/Polyvinylpyrrolidone Polymer Electrolyte Films", *J. Electron Mater.*, vol. 49, pp. 2381–2392, 2020.

[36] M.A. Morsi, A.H. Oraby, A.G. Elshahawy, R.M. Abd El-Hady, "Preparation, structural analysis, morphological investigation and electrical properties of gold nanoparticles filled polyvinyl alcohol/carboxymethyl cellulose blend", *J. Mater. Res. Technol.,* vol. 8(6), pp. 5996–6010, 2019.

[37] M.K. Mishra, S. Moharana, B. Behera, and R.N. Mahaling, "Surface functionalization of $BiFeO_3$: A pathway for the enhancement of dielectric and electrical properties of poly(methyl methacrylate)–$BiFeO_3$ composite films", *Front. Mater. Sci.,* vol. 11 (1), pp. 82–91, 2011.

[38] A.M. El Sayed, W.M. Morsi, "Dielectric Relaxation and Optical Properties of Polyvinyl Chloride/Lead Monoxide Nanocomposites", *Polym. Compos.*, vol. 34, pp. 2031–2039, 2013.

[39] H.M. Ragab, "Spectroscopic investigations and electrical properties of PVA/PVP blend filled with different concentrations of nickel chloride", *Physica B*, vol. 406, pp. 3759–3767, 2011.

Figures

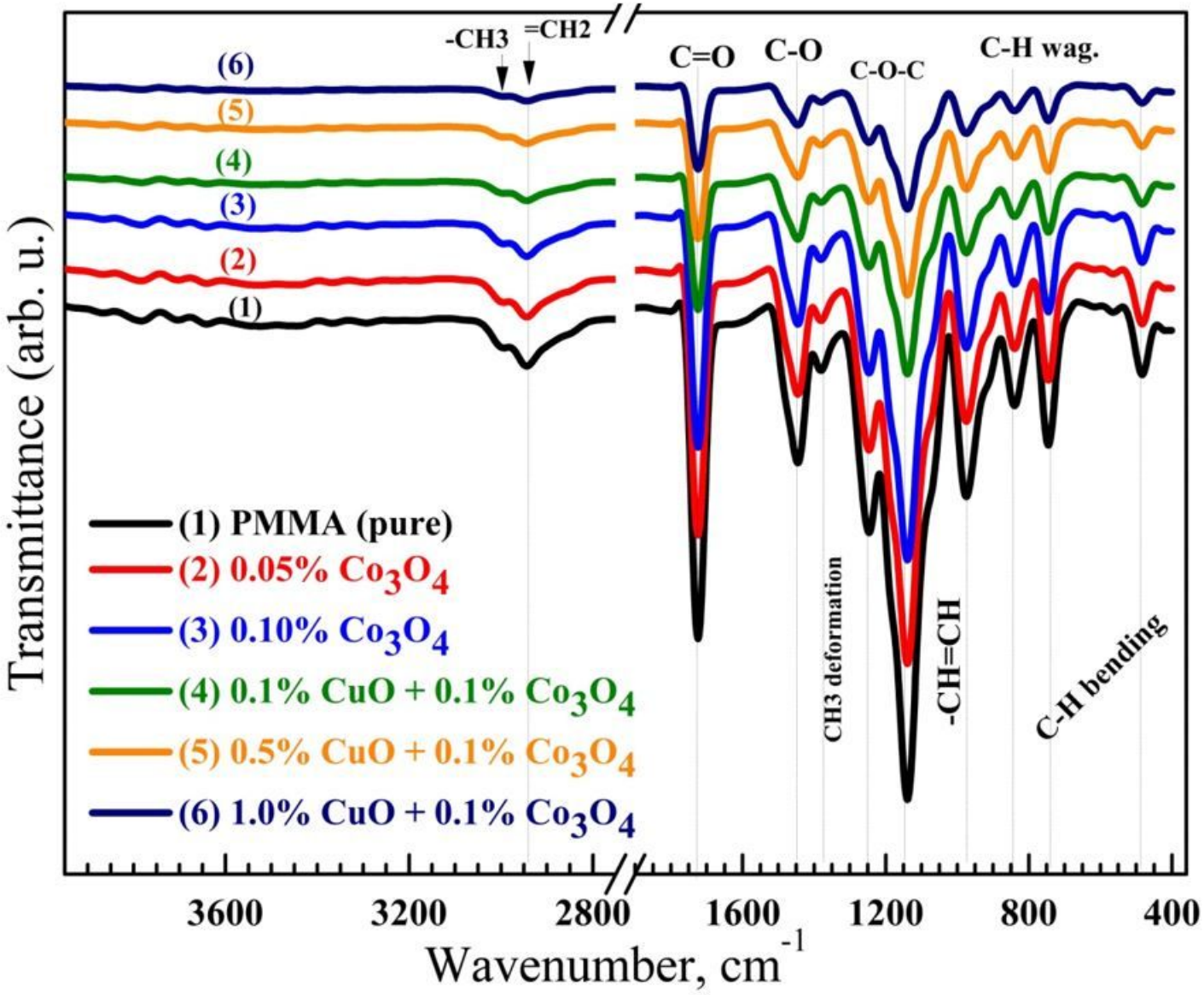

Figure 1

FT-IR spectra of PMMA, PMMA loaded with different amounts of Co3O4 and CuO NPs.

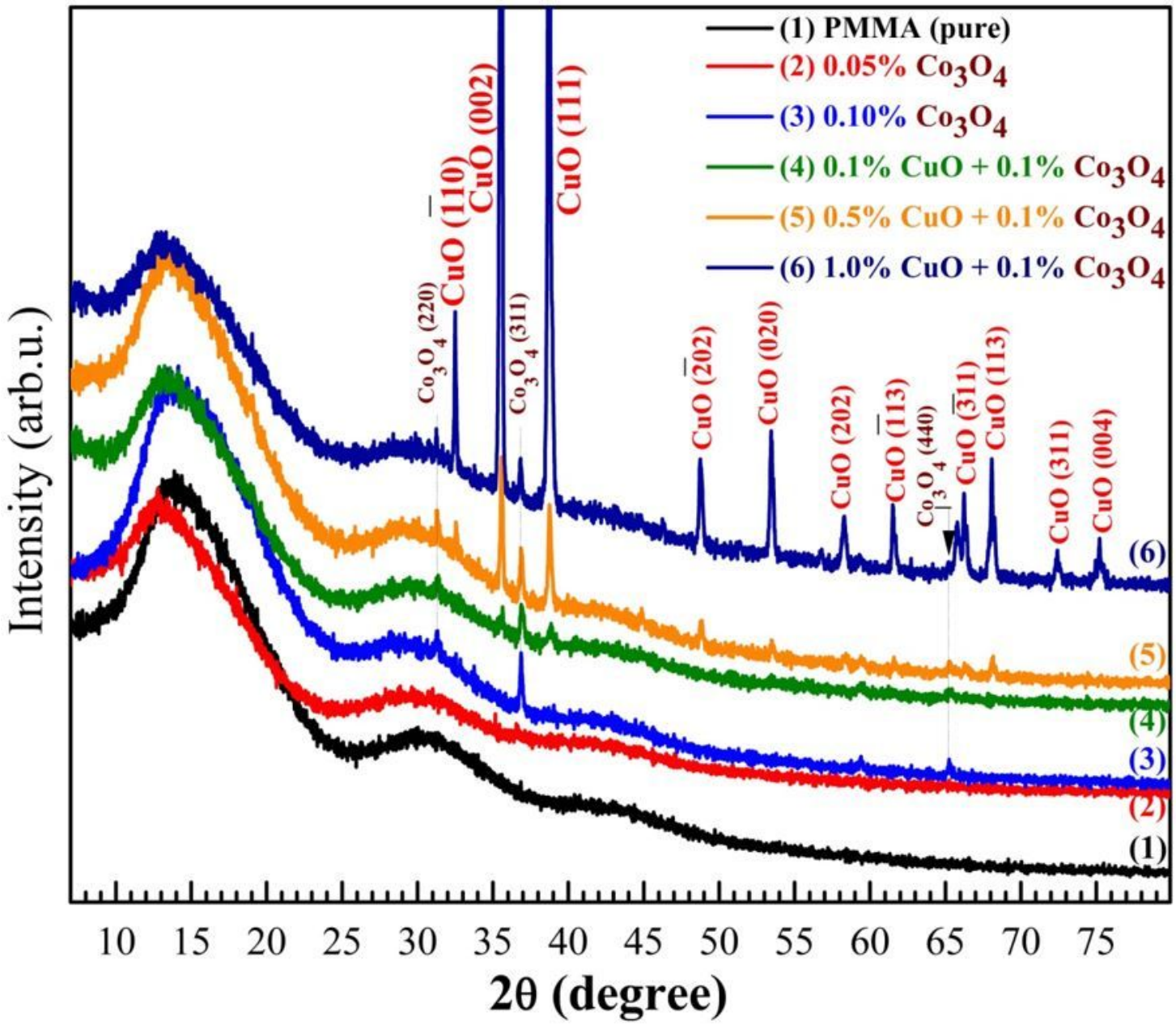

Figure 2

XRD patterns of PMMA, Co3O4/PMMA and CuO/Co3O4/PMMA nanocomposite films.

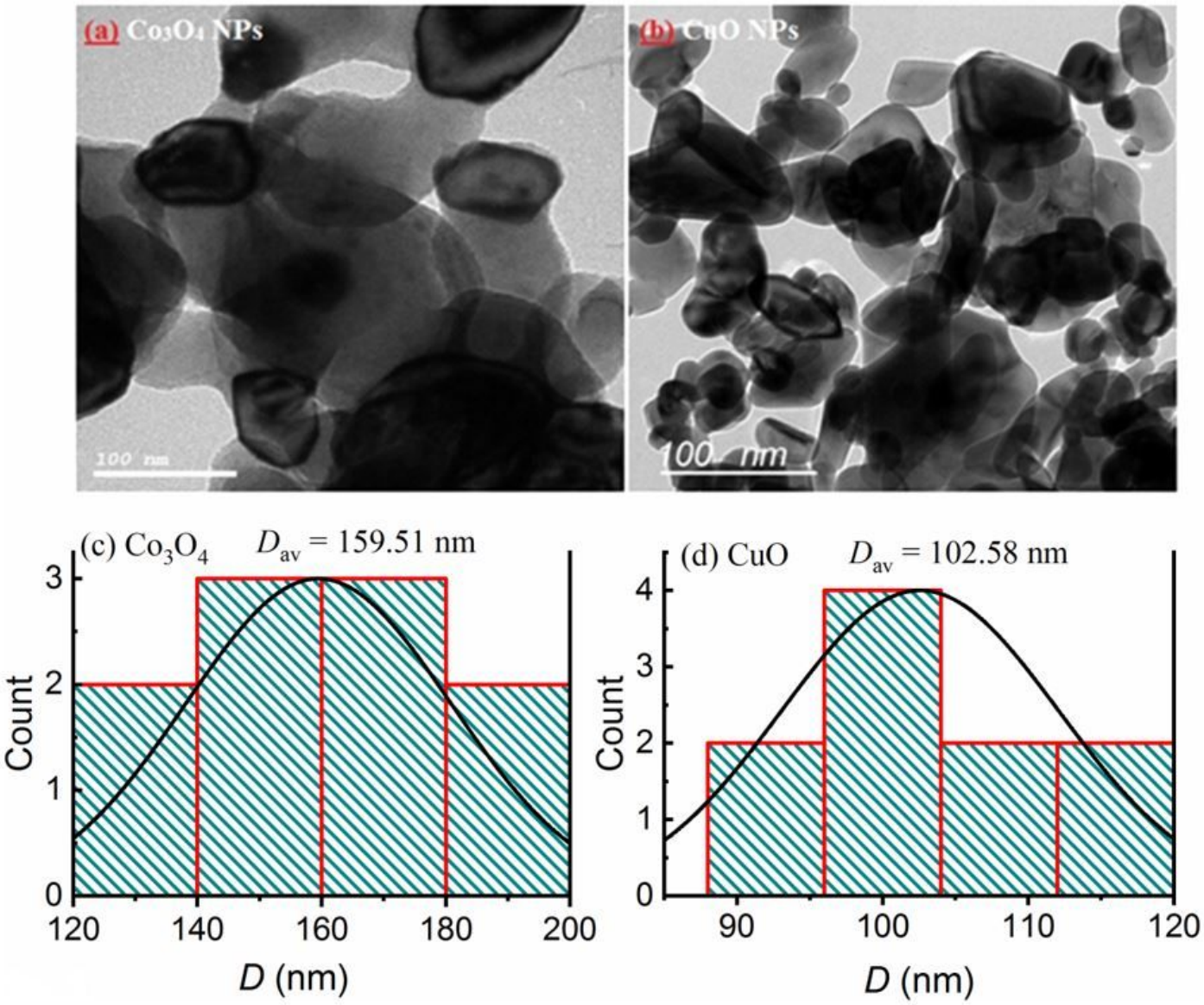

Figure 3

TEM images for (a) Co3O4 and (b) CuO NPs. (c) and (d) are the histograms for the particle size distribution of both two nanooxides.

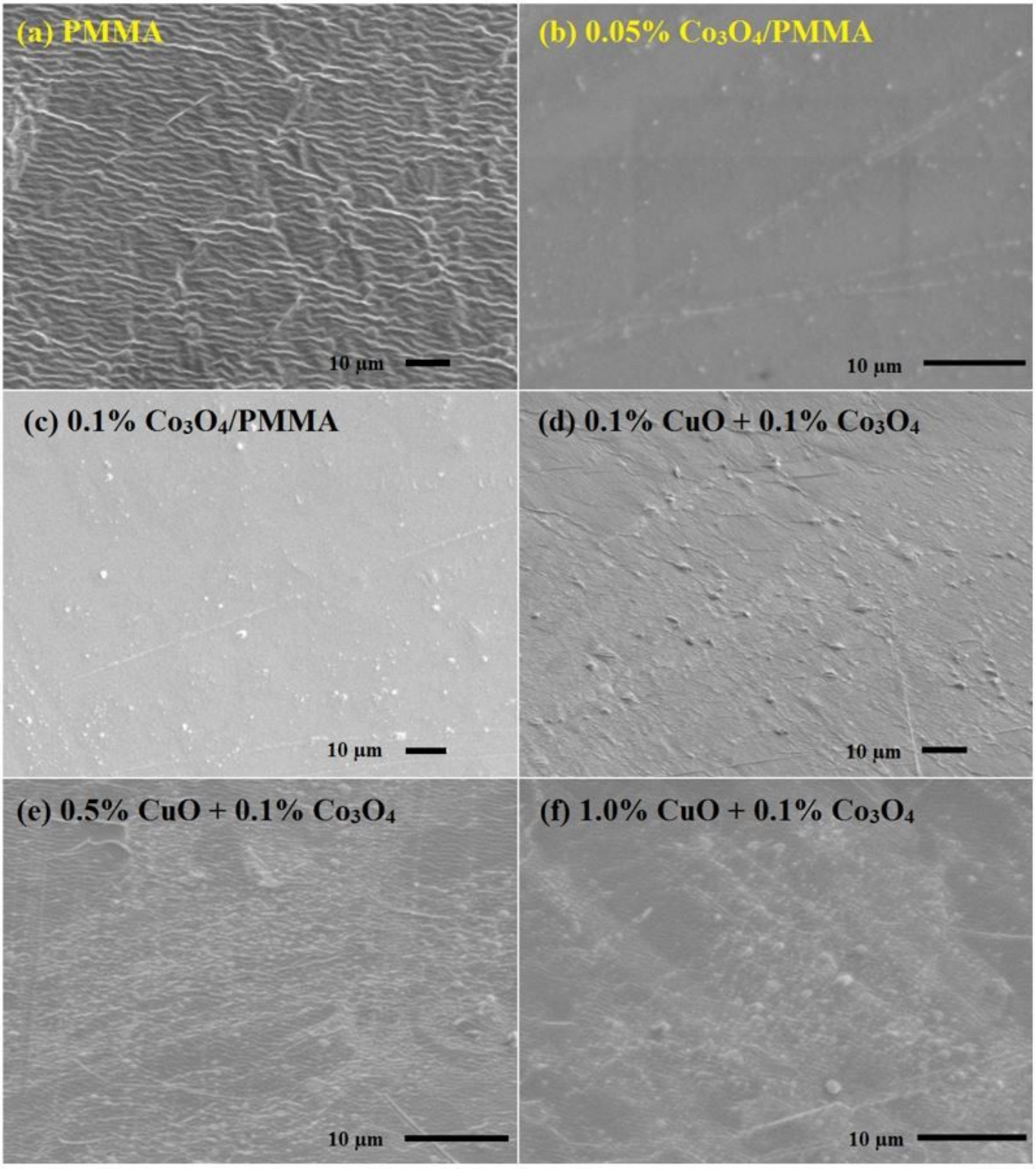

Figure 4

SEM images for (a) PMMA, (b,c) PMMA loaded with Co3O4, and (d-f) Co3O4/PMMA loaded with different amounts of CuO NPs.

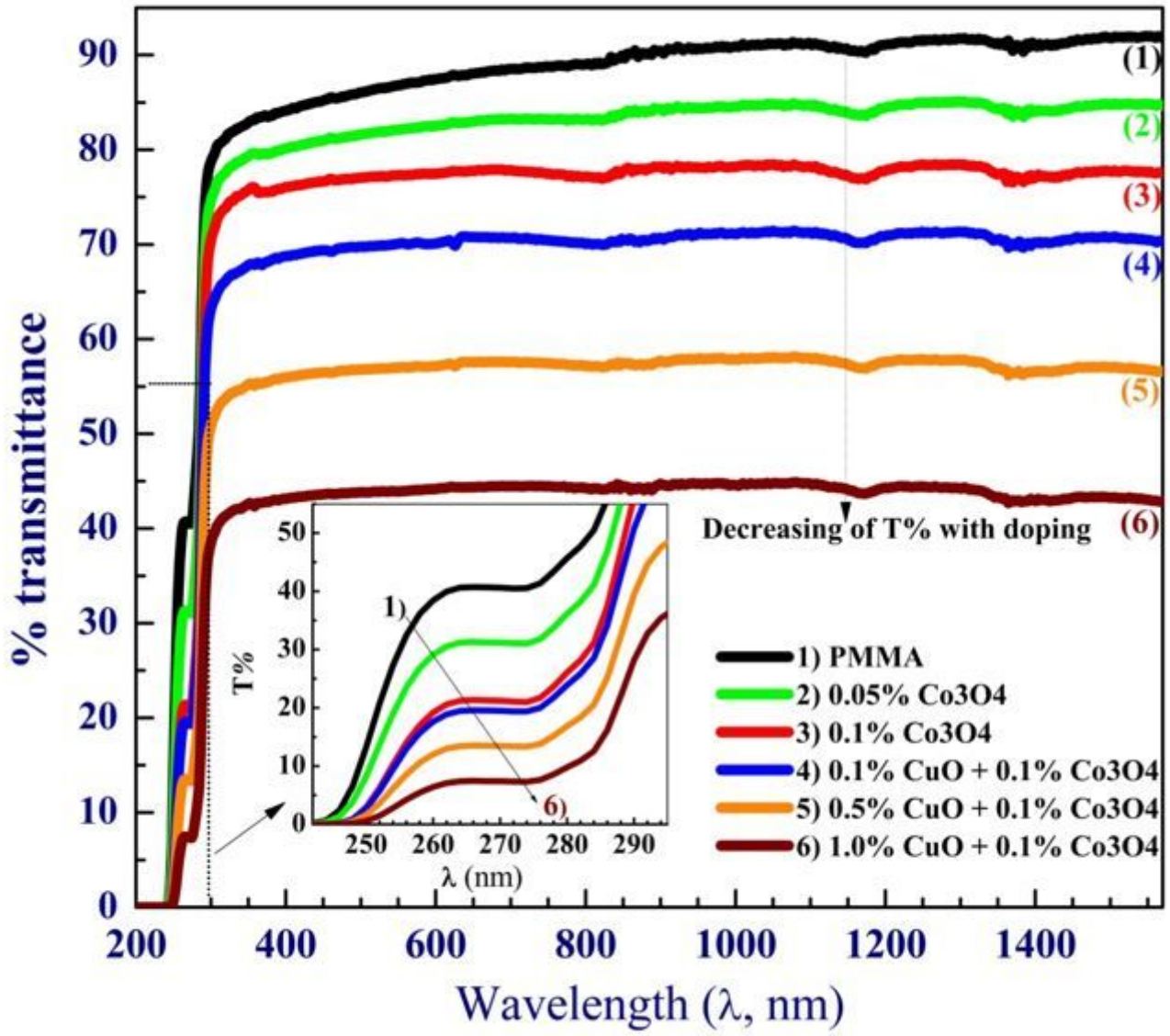

Figure 5

Optical transmittance spectra of PMMA, PMMA loaded with Co3O4 and CuO NPs.

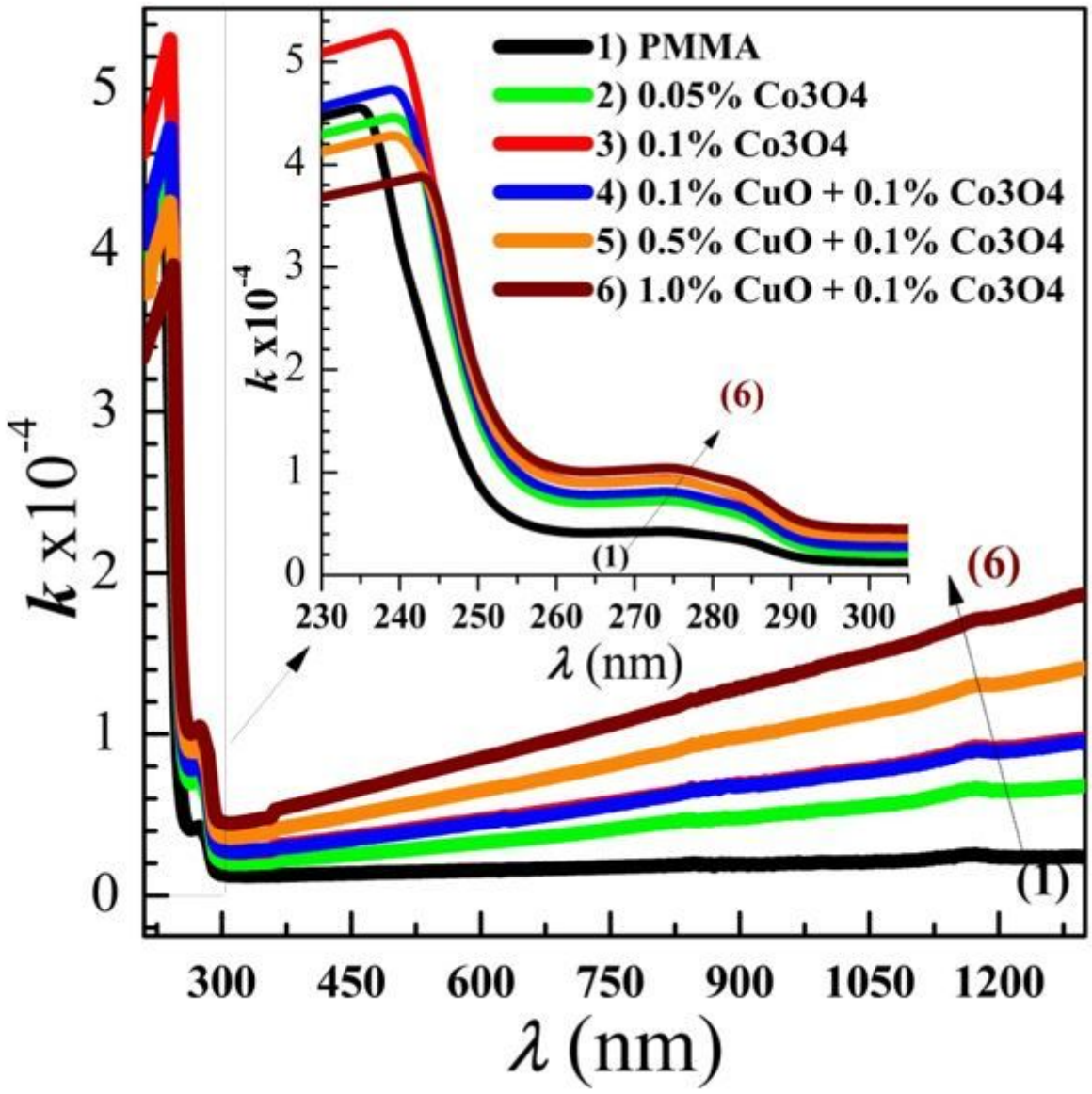

Figure 6

Extinction coefficient distribution of PMMA loaded with Co3O4 and CuO NPs.

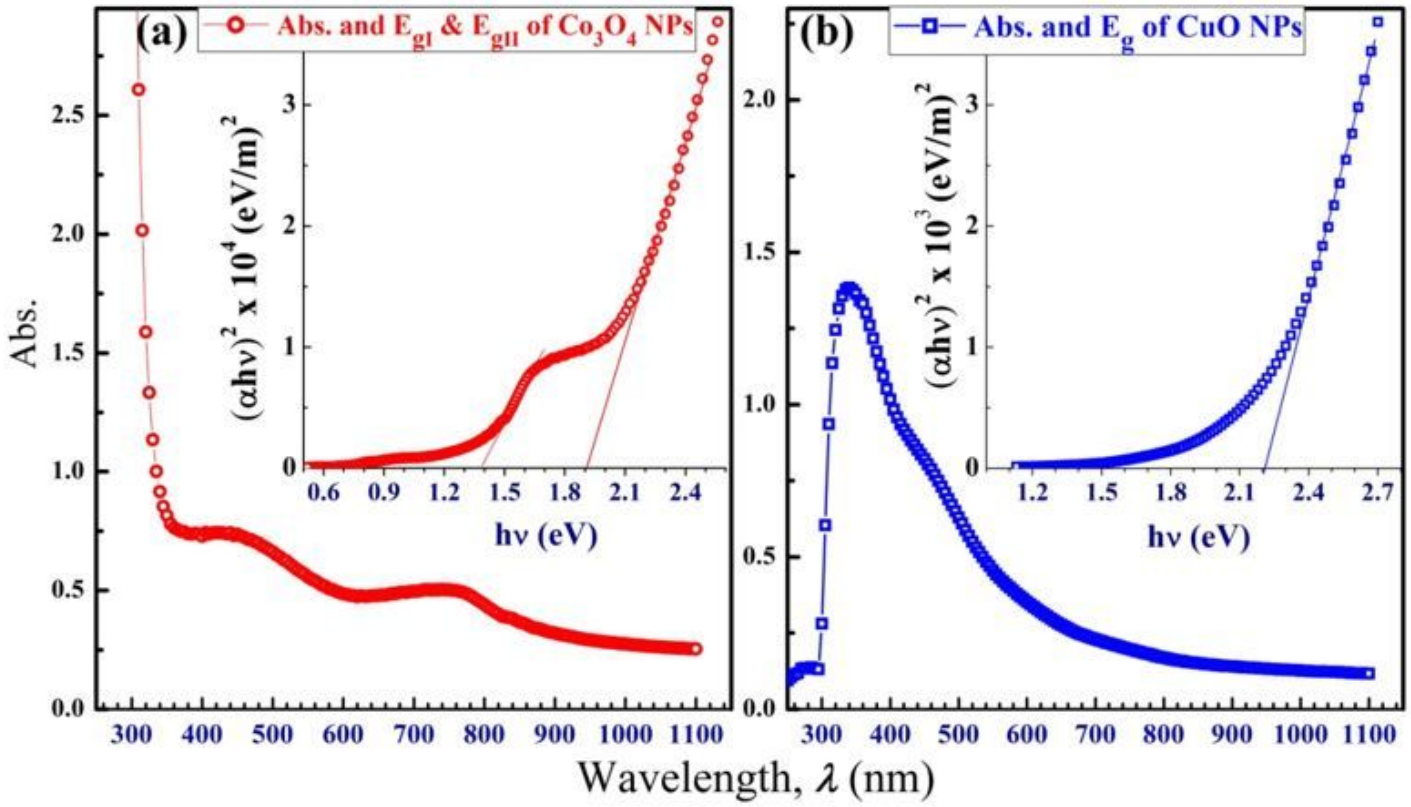

Figure 7

Absorption spectra and Eg calculation for (a) Co3O4 and (b) CuO NPs.

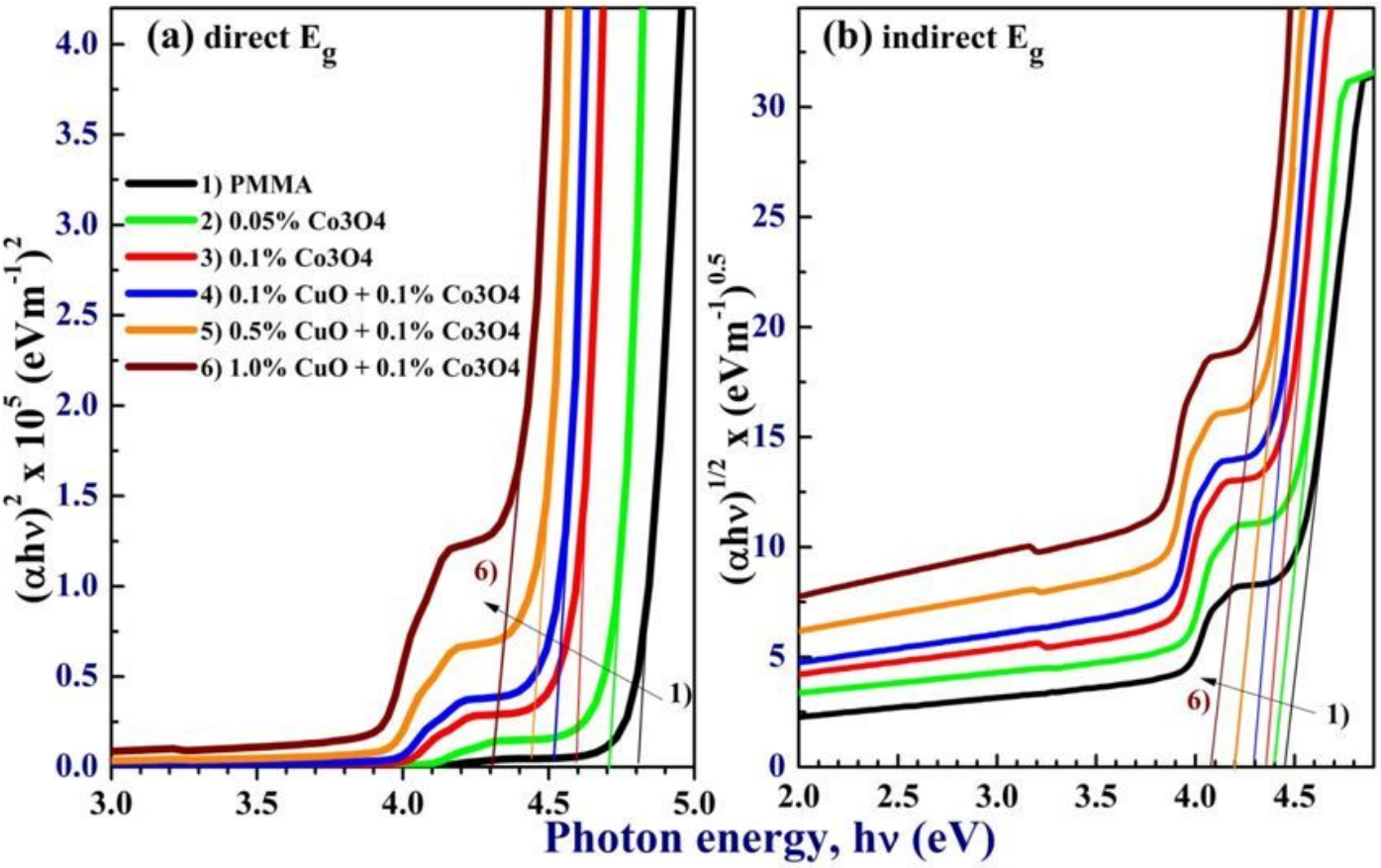

Figure 8

Tauc's plots for (a) direct and (b) indirect energy gap (Eg) of PMMA loaded with Co3O4 and CuO NPs.

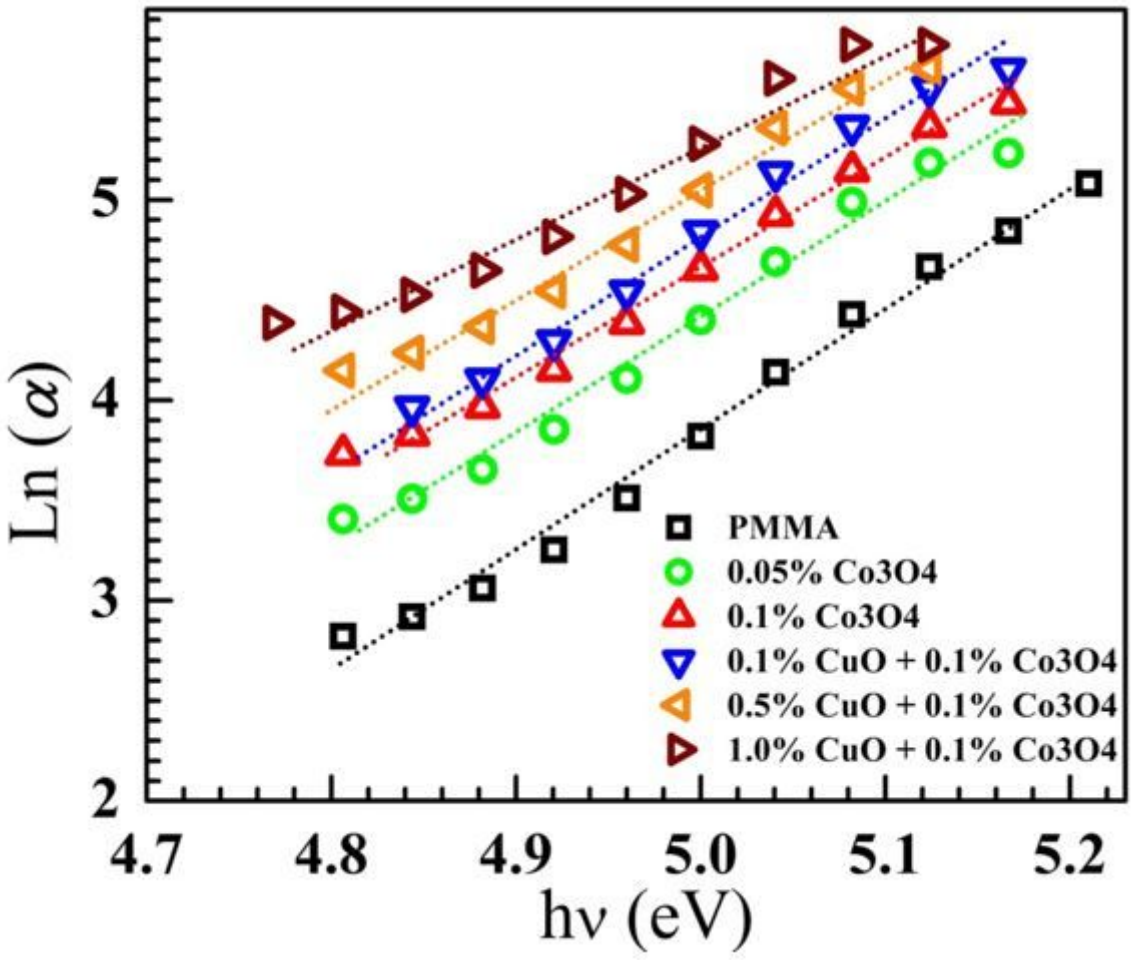

Figure 9

Urbach plot for PMMA and its nanocomposite films.

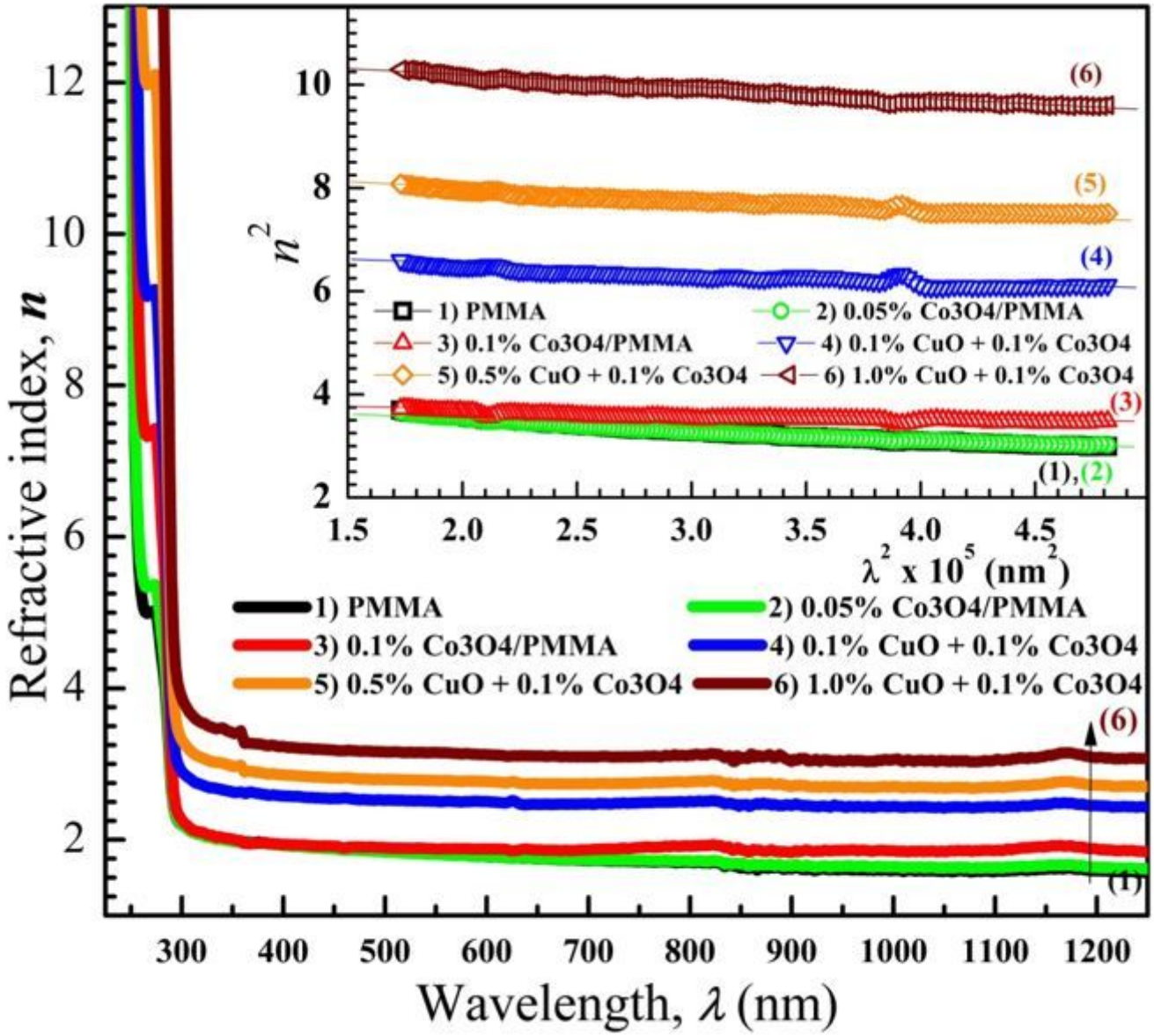

Figure 10

Refractive index of the nanocomposite films and the inset (n2 & λ2) for determination of lattice dielectric constant and carrier concentration to electron effective mass ratio calculation.

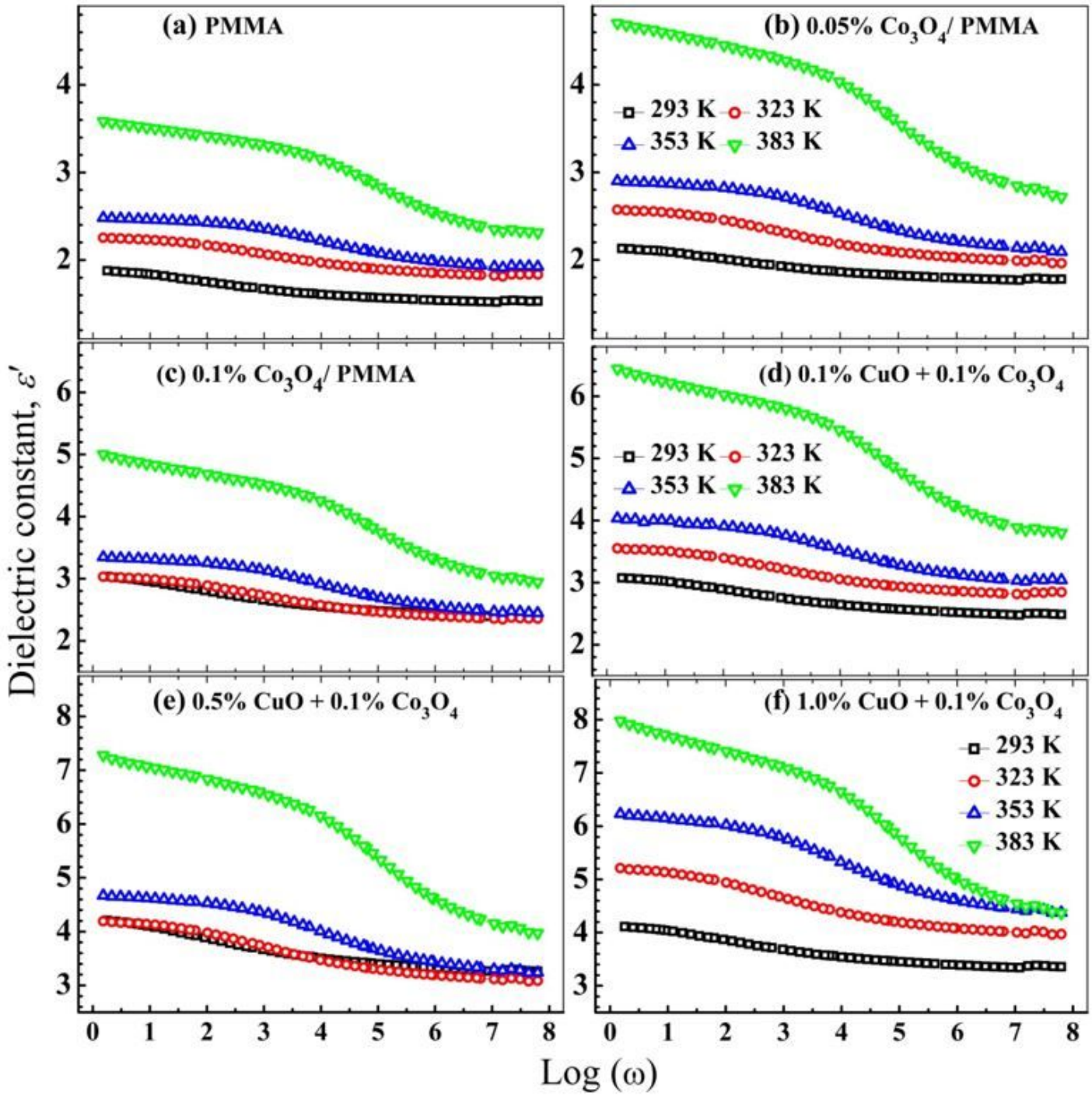

Figure 11

Effect of Co3O4 and CuO of the dielectric constant (ε') of PMMA at different temperatures.

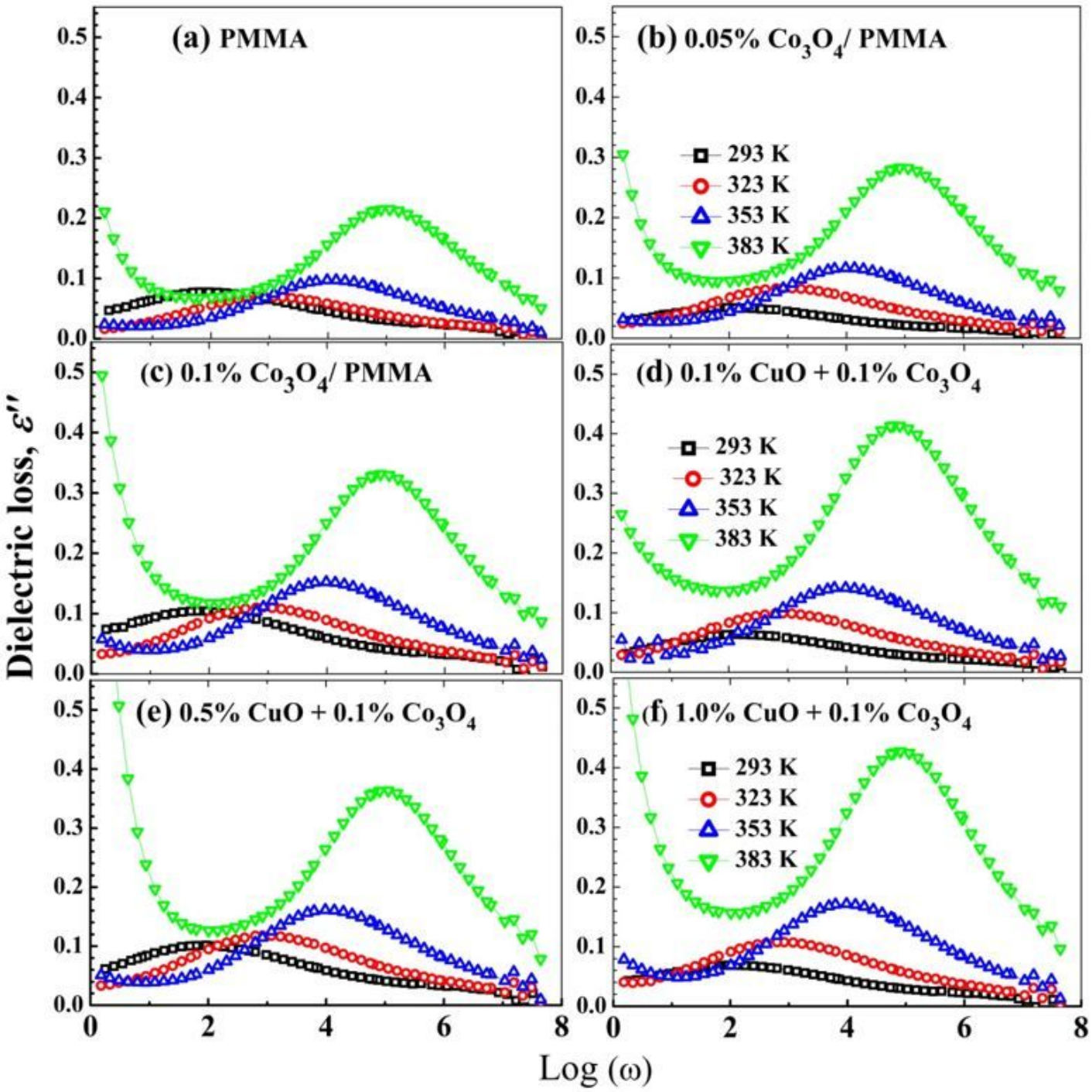

Figure 12

Dielectric loss (ε") of the PMMA and its nanocomposite films at different temperatures.

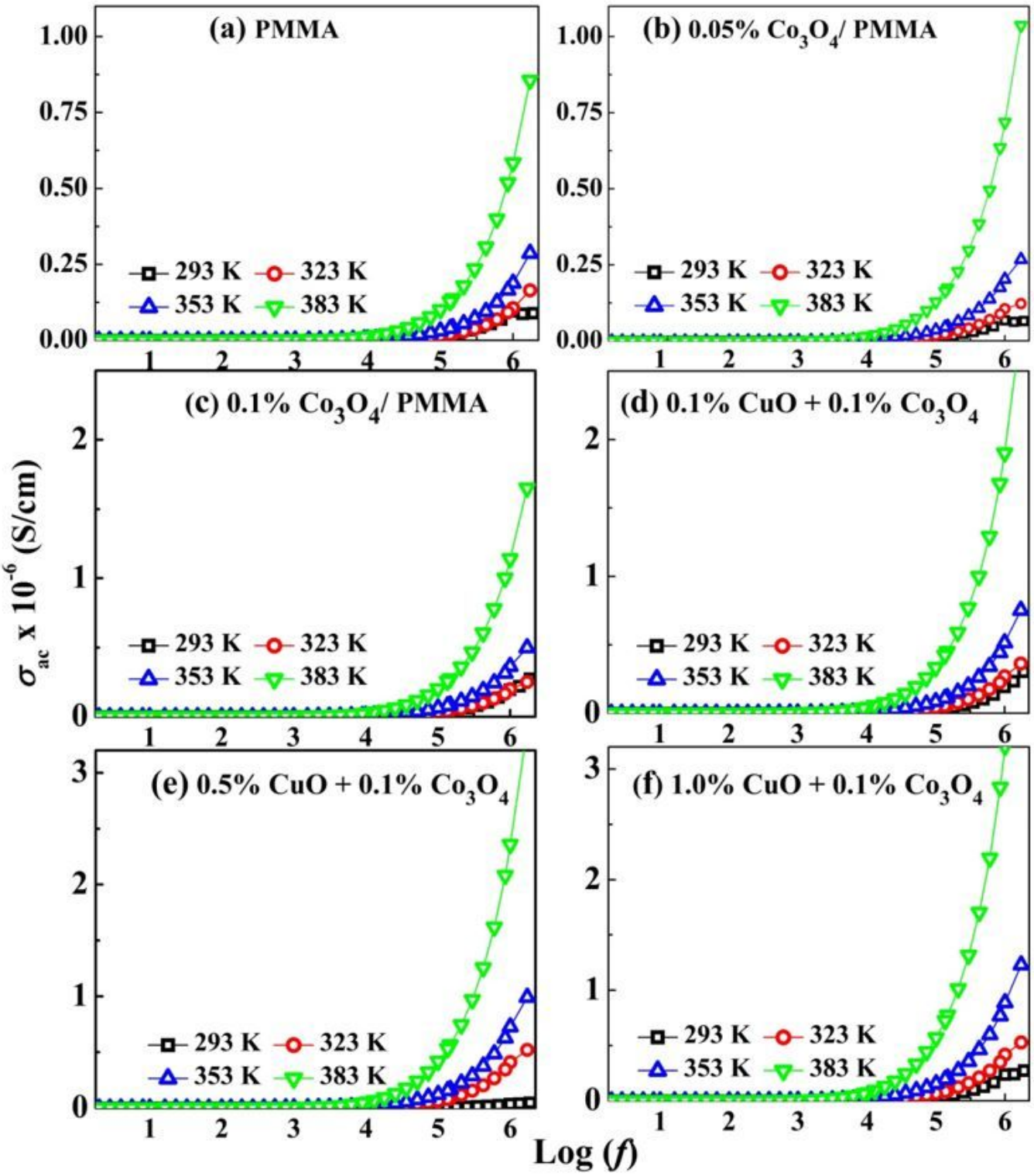

Figure 13

The electric conductivity of PMMA, Co3O4/PMMA and CuO/Co3O4/PMMA films at different temperatures.

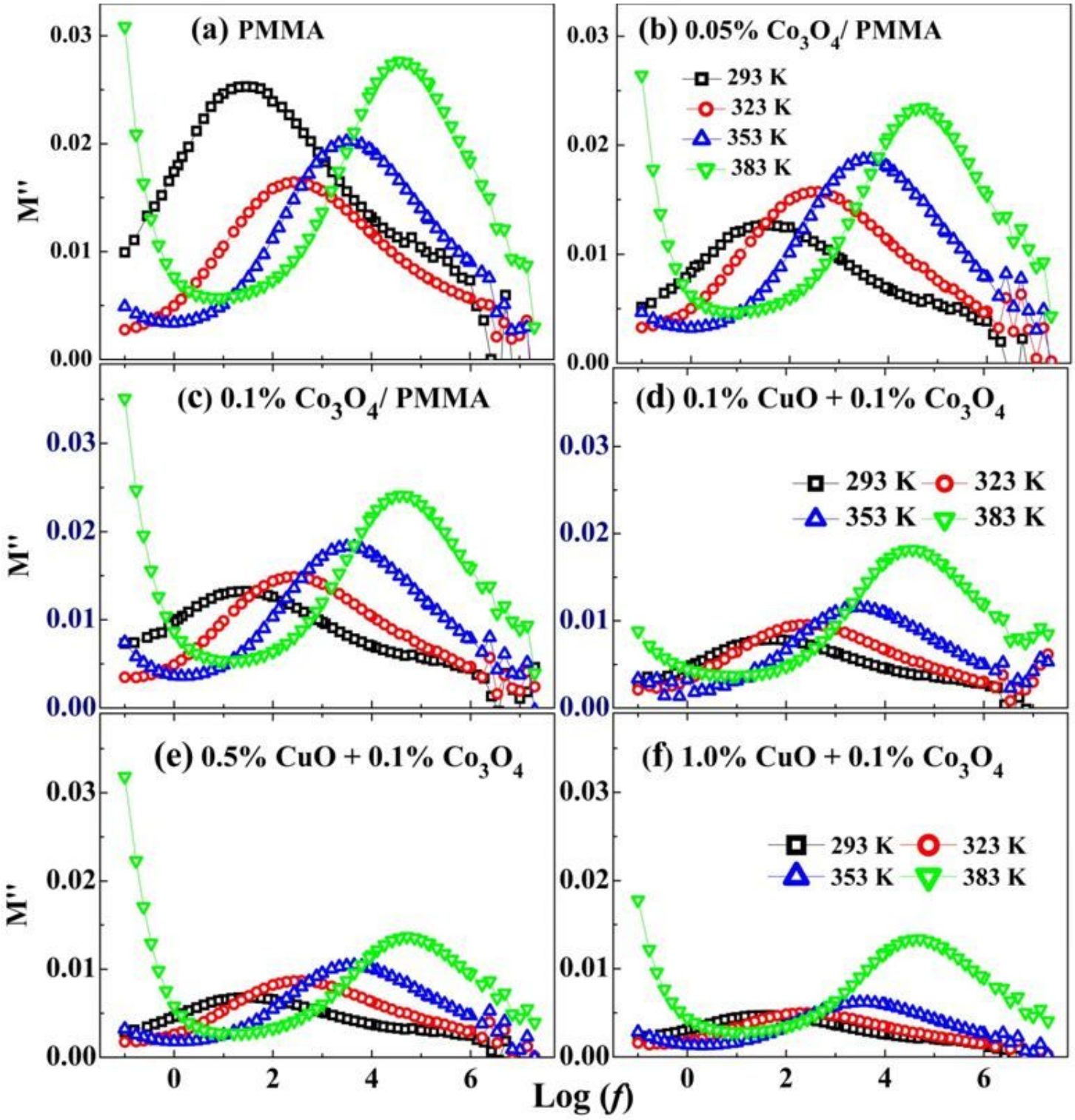

Figure 14

Imaginary dielectric modulus (M") of the PMMA and its nanocomposite films.

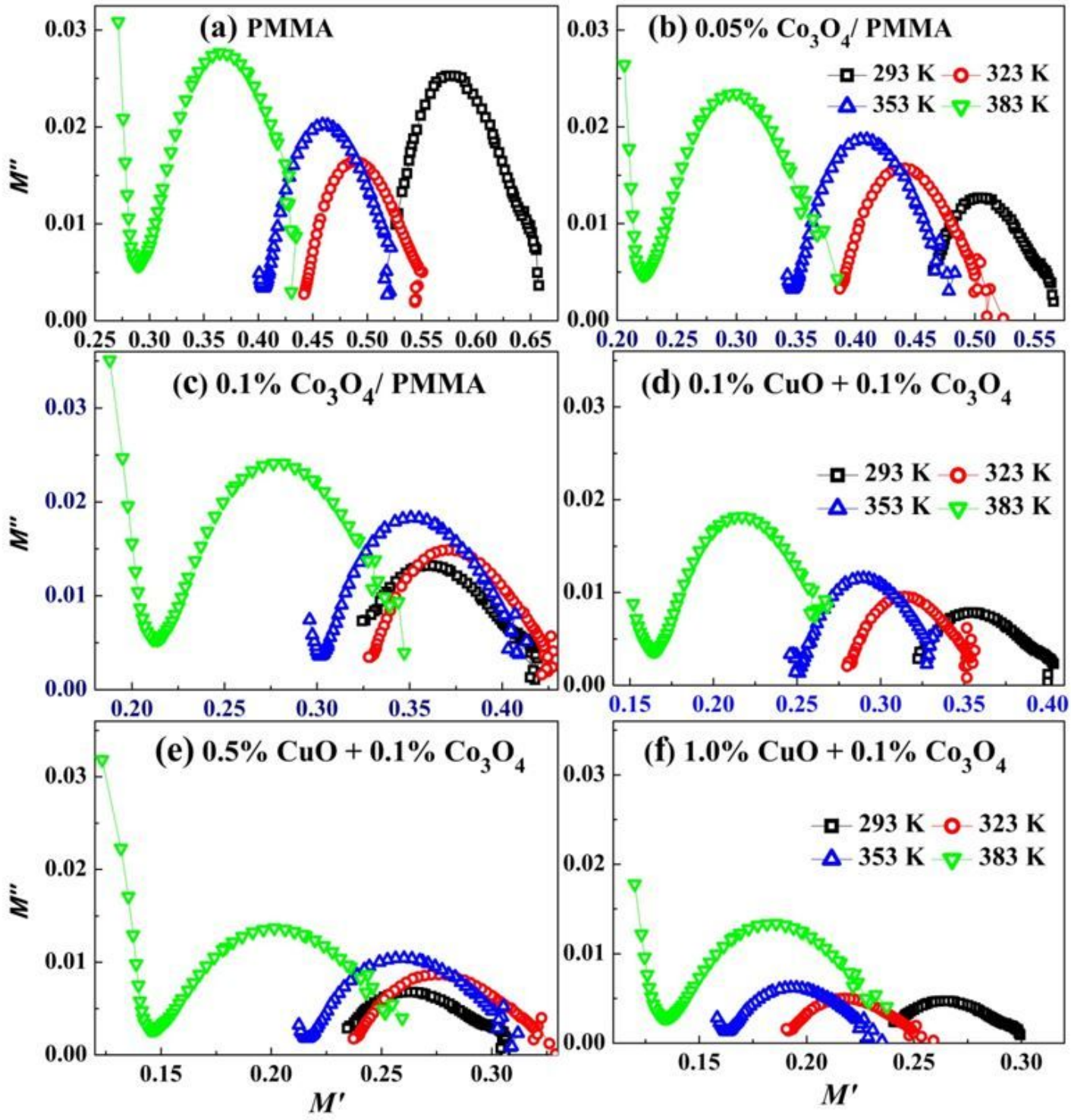

Figure 15

Argand's plot for the nanocomposite films at four different temperatures.